Chapter IV

Entatic Effects on the Photophysical Processes in Copper Photosensitizers

Introduction

The ability to control the functional properties of transition metal coordination complexes is critical to our understanding and implementation of transition metal catalysts, photosensitizers, and metalloenzymes. Although many of the electronic properties of transition metal centers are determined first by the identity of the metal, oxidation state, and ligand-field symmetry of the inner coordination sphere, secondary coordination sphere effects including sterics may significantly impact the ground and excited state potential energy surfaces. Such an effect is observed in biology where the fold of a protein, long range hydrogen bonding, and electrostatics can serve to distort the ligand field at the metal site. The metal center may thus persist in an otherwise energetically activated geometry, known as the entatic or rack-induced state.[1–15]

In analogy to the entatic state observed in some metalloproteins, secondary coordination sphere steric effects have been detailed in small molecule coordination complexes, notably in Cu(I) bis-phenanthrolines (bis-phen).[16–25] Cu(I) bis-phen complexes have garnered interest for their potential uses as first-row transition metal photosensitizers and thermally activated delayed fluorescence emitters. Cu(I) bis-phen complexes exhibit a pseudo-tetrahedral ground state geometry. The visible absorption spectrum of Cu(I) bis-phen complexes is typically dominated by metal-to-ligand charge transfer (MLCT) transitions.[17,18,20,23] Absorption into the ^{1}MLCT state generates a transient, formally Cu(II) center. Cu(II) is destabilized in a tetrahedral coordination environment and will tend to undergo Jahn-Teller tetragonal distortions towards a planar geometry, as illustrated in Figure 4.1. Intersystem crossing (ISC) then permits formation of a long-lived ^{3}MLCT state. Steric restraints can be introduced at the 2- and 9-positions on the phenanthroline moiety that attenuate the degree of flattening that occurs in the excited state. As a result, the reorganization/excited state relaxation energies may be modulated, and the resulting excited state lifetimes of the ^{3}MLCT state can be tuned over orders of magnitude.

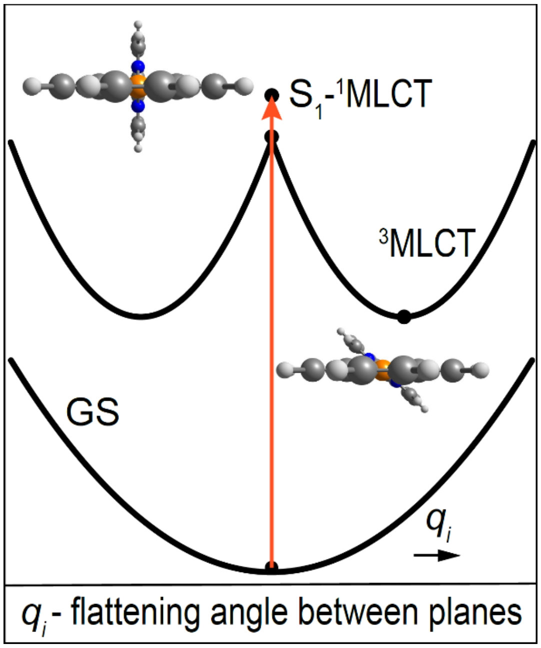

Figure 4.1 ^{3}MLCT excited state structural distortion in Cu(I) bis-phenanthroline complexes and their generalized excited state potential energy surfaces. The steric effects under consideration here inhibit the flattening of the dihedral angle upon formation of the ^{3}MLCT excited state.

In this study we attempt to quantify the steric contributions to the ground and excited state potential energies surfaces involved in a range of Cu(I) bis-phen complexes by combined computational and experimental methods. In doing so, we demonstrate that the trends in the excited state lifetimes with respect to ligand sterics are rationalized in terms of the energy gap law.[26,27] We will initially focus on the experimental contributions made to the project as a part of this thesis, which include synthesis, cyclic voltammetry, steady-state absorption and emission spectroscopy, as well as transient absorption (TA) spectroscopy to validate the computationally observed trends in reduction potential and ^{3}MLCT lifetimes in the context of previous work on such complexes. We will then summarize the computational work that comprised the core of the study.

Experimental Results

To the goal of providing benchmark characterization of Cu(I) bis-phen complexes for the computational studies in this work, we focused our attention on several 2,9-dialkyl-substituted Cu(I) bis-phen complexes with increasing steric bulk in the 2,9-positions. $[Cu(phen)_2][PF_6]$[28], $[Cu(dmp)_2][PF_6]$[29], and $[Cu(dsbp)_2][PF_6]$[28] were synthesized according to literature procedures (dmp = 2,9-dimethyl-1,10-phenanthroline, dsbp = 2,9-di-*sec*-butyl-1,10-phenanthroline). We report here the synthesis and characterization of the related Cu(I) complex of 2-methyl-1,10-phenanthroline ($[Cu(mmp)_2][PF_6]$).[30] The key parameters we targeted for benchmarking are the ground state reduction potential for the Cu(I/II) couple ($E°$), the excited state relaxation energies (γ), and the ^{3}MLCT excited state lifetimes (τ). Cyclic voltammetry was performed to assess the Cu(I/II) reduction potential of the complexes. Gaussian fitting of low temperature emission data provides access to excited state relaxation energies via the fitted full-width half-maxima (FWHM) of the Gaussian bands.[31] Finally, transient absorption allows us to track the excited state dynamics of the complexes and measure the excited state lifetimes.

Synthesis of $[Cu(mmp)_2][PF_6]$

$[Cu(mmp)_2][PF_6]$ was synthesized according to a modified literature procedure.[30] A solution of 2-methyl-1,10-phenanthroline (194.2 mg, 1.0 mmol) in MeCN (3 mL) was added to $[Cu(MeCN)_4][PF_6]$ (186.4 mg, 0.5 mmol) under $N_{2(g)}$ atmosphere. The deep red solution was then stirred for fifteen minutes and Et_2O (~20 mL) was added to precipitate the product, which was then recrystallized via slow vapor diffusion of Et_2O into a concentrated DCM solution of the product.

The resulting crystals were collected and washed with Et_2O, yielding the product (near quantitative yield). ^1H NMR (400 MHz, $CDCl_3$): δ 2.48 (s, 6H), 7.81 (d, 2H), 7.88 (dd, 2H), 8.06 (m, 4H), 8.50 (d, 2H), 8.57 (d, 2H), 8.86 (d, 2H), ppm. ^{13}C NMR (400 MHz, $CDCl_3$) δ 25.99, 125.29, 125.94, 126.16, 127.06, 127.46, 129.59, 137.03, 137.24, 143.31, 143.71, 148.81, 158.02 ppm.

Cyclic Voltammetry

The Cu(I/II) reduction potential for $[Cu(phen)_2][PF_6]$, $[Cu(dmp)_2][PF_6]$, and $[Cu(mmp)_2][PF_6]$ were estimated using cyclic voltammetry (CV). CV was carried out with a Pine Instrument Company AFCBP1 biopotentiostat with the AfterMath software package. Measurements were performed in a three electrode cell, consisting of a glassy carbon working electrode (⌀ = 3.0 mm), a silver wire counter electrode, and a platinum wire reference electrode under a $N_{2(g)}$ atmosphere at room temperature in an M. Braun glovebox. Cyclic voltammograms were taken of 2 mM solutions of Cu bis-phen complex and 0.1 M $[Bu_4][PF_6]$ electrolyte in dry dichloromethane. The ferrocene/ferrocenium (Fc/Fc^+) redox couple or alternatively the decamethylferrocene/decamethylferrocinium (Fc^*/Fc^{*+}) redox couple were used as internal reference standards for all measurements. Those redox potentials referenced to Fc^*/Fc^{*+} could then be converted to potentials vs. Fc/Fc^+ by using the measured difference in redox potentials of the Fc^*/Fc^{*+} and Fc/Fc^+ under our conditions.[32,33]

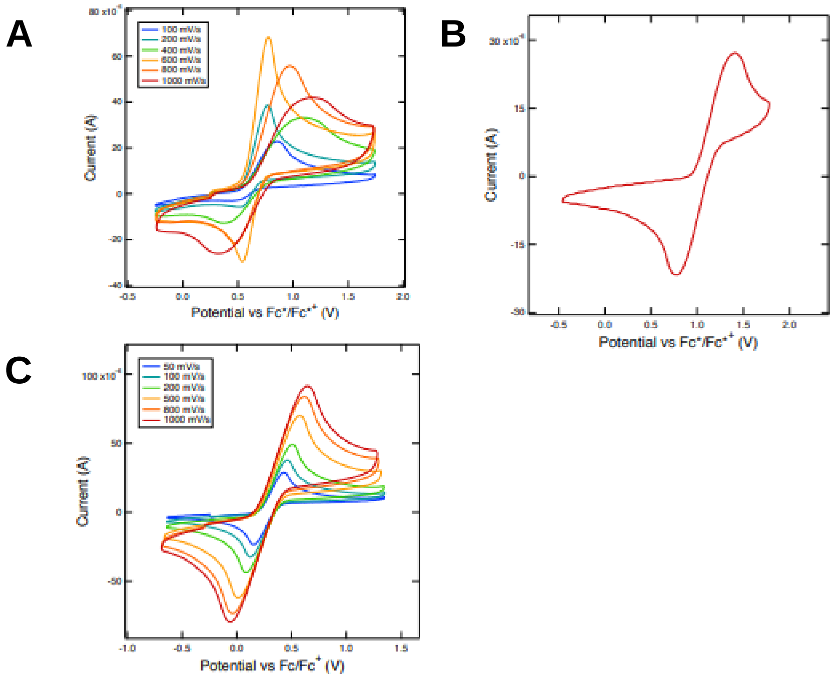

Figure 4.2 Electrochemical data (CVs) for a variety of Cu(I) bis-phen complexes. **(A)** scan rate dependence of [Cu(phen)$_2$][PF$_6$] referenced vs Fc*/Fc*$^+$; **(B)** CV data for [Cu(dmp)$_2$][PF$_6$] referenced vs Fc*/Fc*$^+$; **(C)** scan rate dependence for [Cu(mmp)$_2$][PF$_6$] referenced vs Fc/Fc$^+$.

The CV data collected on [Cu(phen)$_2$][PF$_6$] (scan rate dependence), [Cu(dmp)$_2$][PF$_6$] (CV), and [Cu(mmp)$_2$][PF$_6$] (scan rate dependence) are presented in Figure 4.2. Although [Cu(dmp)$_2$][PF$_6$] and [Cu(mmp)$_2$][PF$_6$] exhibit cleanly reversible Cu(I/II) redox events, [Cu(phen)$_2$][PF$_6$] requires high scan rates to display relatively reversible CV features. Addition of ferrocene allows us to reference the reduction potential of each complex versus the ferrocene/ferrocenium couple. We convert these values versus NHE to compare across complexes reported in the literature as shown in Table 4.1.

77 K Luminescence Experiments

77 K emission spectra were collected in the Beckman Institute Laser Resource Center using a modified Jobin Yvon Spec Fluorolog-3 instrument employing two Ocean Optics EQDPro CCD spectrometers spanning 300 – 930 nm for detection. Samples run were 1 mM solutions of $[Cu(dsbp)_2][PF_6]$, $[Cu(dmp)_2][PF_6]$, and $[Cu(mmp)_2][PF_6]$ in 1:1 toluene/dichloromethane after being degassed by sparging with $N_{2(g)}$ for 10 minutes. Samples were added to an EPR tube and glassed at 77 K in liquid N_2. The sample compartment of the fluorimeter was purged with $N_{2(g)}$ for 10 min prior to introduction of the sample. The glassed samples were then transferred to a vacuum-sealed double-walled glass Dewar containing liquid N_2. Samples were excited with a xenon arc lamp, employing a monochromator for wavelength selection, and emission was collected at 90 °. Once collected, emission spectra were fit to a minimum of three Gaussian peaks of equal full-width half-maximum using nonlinear least squares estimation of the coefficients with the nonlinear regression fitting package in MATLAB. The excited state relaxation energy was then calculated from the fitted full-width half-maximum values.

The collected 77 K emission spectra for $[Cu(dsbp)_2][PF_6]$, $[Cu(dmp)_2][PF_6]$, and $[Cu(mmp)_2][PF_6]$ are shown in Figure 4.3 along with the Gaussian fitting obtained from the data. Emission at 77 K could not be observed for $[Cu(phen)_2][PF_6]$.[31]

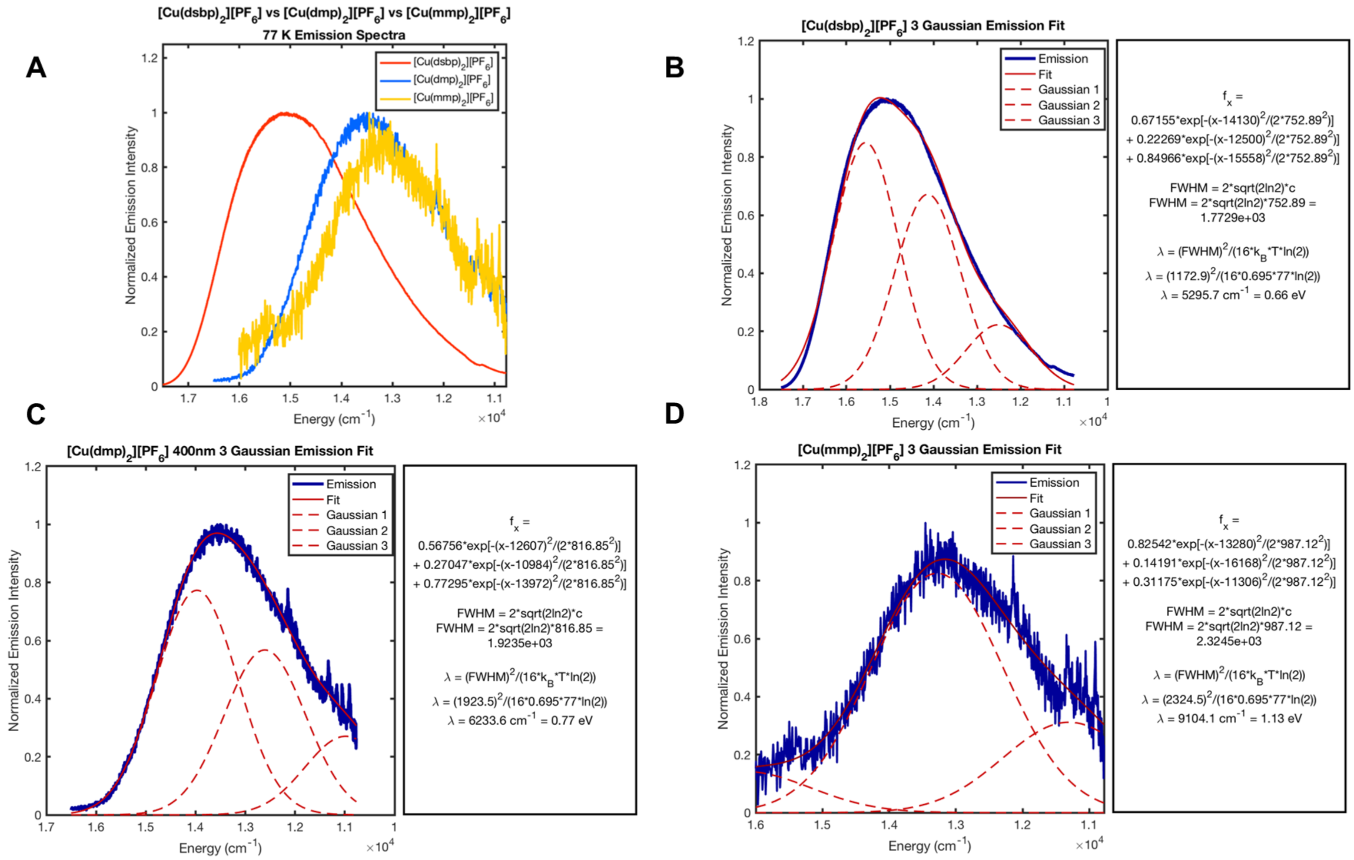

Figure 4.3 77 K emission spectra collected for [Cu(dsbp)$_2$][PF$_6$], [Cu(dmp)$_2$][PF$_6$], and [Cu(mmp)$_2$][PF$_6$] with 400 nm excitation with **(A)** normalized emission spectra of the three complexes overlayed with each other and the emission profile of **(B)** [Cu(dsbp)$_2$][PF$_6$], **(C)** [Cu(dmp)$_2$][PF$_6$], and **(D)** [Cu(mmp)$_2$][PF$_6$] fitted to a sum of three Gaussian curves (total fit shown in solid red, individual curves in dashed red).

In Figure 4.3A the overlay of the normalized emission traces shows a blue shift in the emission maximum λ_{max} with increasing steric bulk in the 2,9-positions of the phenanthroline (dsbp > dmp > mmp). The signal-to-noise ratio also improves with increasing bulk due to overall higher emission intensity. This is consistent with previous literature. As the increasing bulk prevents relaxation of the ^{3}MLCT into a tetragonal geometry, this potential energy surface is displaced higher in energy relative to the ground state, resulting in higher energy emission. The excited state relaxation parameters acquired via Gaussian fitting also support this: dsbp (0.66 eV) < dmp (0.77 eV) < mmp (1.13 eV). As the steric bulk hinders relaxation into the tetragonal geometry, the excited state relaxation energy will be less for bulkier substituents.

Steady-State and Transient Absorption Spectroscopy

In order to characterize the optical properties $[Cu(mmp)_2][PF_6]$, we collected steady-state absorption spectra as well as transient absorption spectra. We present the steady-state absorption data in Figure 4.4, performing Beer-Lambert analysis to ascertain the extinction coefficient at the λ_{max} of the MLCT absorption band at 455 nm.

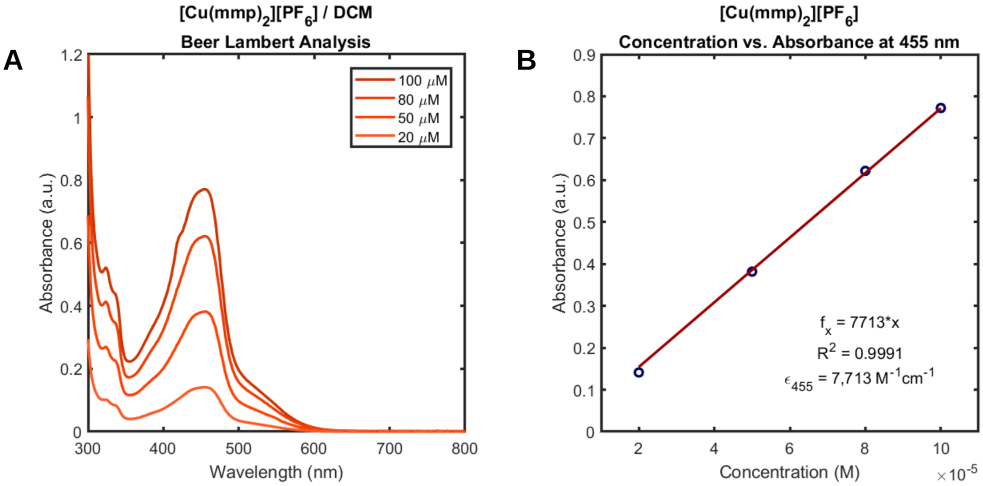

Figure 4.4 (A) Concentration dependent visible absorption spectra for $[Cu(mmp)_2][PF_6]$ in DCM **(B)** Concentration dependent absorbance at 455 nm and linear fit to extract the extinction coefficient.

Ultrafast transient absorption spectroscopy was acquired on the $[Cu(mmp)_2][PF_6]$ sample with excitation at 410 nm. The spectra are shown in Figure 4.5 along with single wavelength kinetic fitting to ascertain the ^{3}MLCT excited state lifetime.

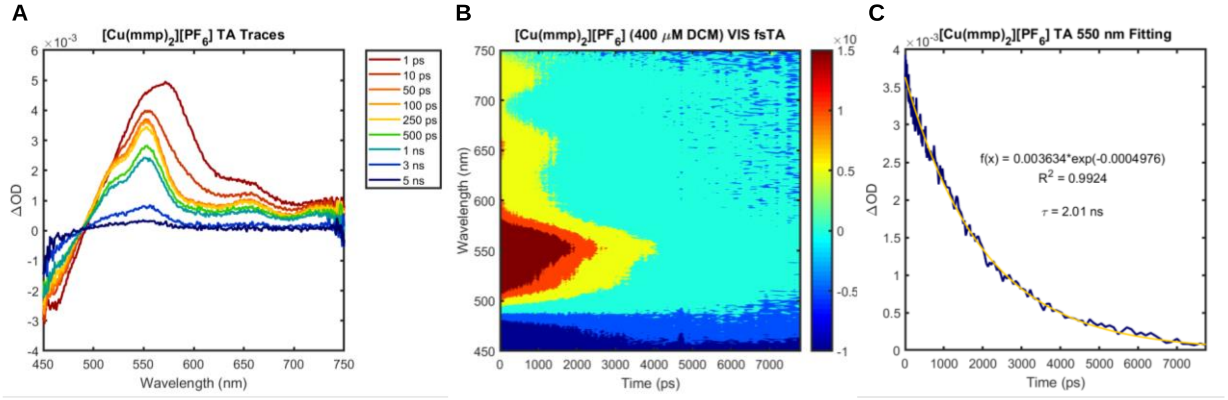

Figure 4.5 (A) Time cuts of the fsTA spectrum of $[Cu(mmp)_2][PF_6]$ in DCM showing the spectral evolution over time; **(B)** a 2D plot of the data matrix over the time course of the instrument; **(C)** Single wavelength exponential fitting at 550 nm after the initial ~50 ps to extract the ^{3}MLCT lifetime τ.

The time cuts of the fsTA spectrum show an excited state absorption (ESA) feature in the visible region spanning 500 – 750 nm. Over the first tens of picoseconds, the broad ESA blue shifts and sharpens into a long-lived ESA feature. This is consistent with previous TA experiments on Cu(I) bis-phen complexes, and the long-lived feature is consistent with the ^{3}MLCT state. We fit the long-lived component near its maximum at 550 nm at times after the broad ESA feature blue shifts to the long-lived ESA (~50 ps). This gives us a ^{3}MLCT excited state lifetime $\tau = 2.01$ ns.

Computational Results

2,9-Alkyl Substituted Copper(I) Bis-phenanthrolines

The reduction potentials ($E°$s) and ^{3}MLCT excited state lifetimes (τ) for a variety of Cu(I) bis-phen complexes have been reported in the literature.[17,18,23,31,34–38] Among these are six homoleptic Cu(I) bis-phen complexes differing only in the alkyl group at the 2,9-position of the phenanthroline ligand (*viz*., 1,10-phenanthroline (phen), 2,9-dimethyl-1,10-phenanthroline (dmp), 2,9-dibutyl-1,10-phenanthroline (dbp), 2,9-dineopentyl-1,10-phenanthroline (dnpp), 2,9-di-*sec*-butyl-1,10-phenanthroline (dsbp), and 2,9-di-*tert*-butyl-1,10-phenanthroline (dtbp)). Solely changing the alkyl group at the 2,9-positions tunes the Cu(I/II) $E°$ over ~600 mV and ^{3}MLCT lifetimes by greater than four orders of magnitude (e.g., from 140 ps (bis-phen) to 3.26 μs (bis-dtbp) in DCM).[18] These systematic structure/function variations thus provide an opportunity to quantify steric contributions in photophysical processes. Indeed, our examination of these complexes demonstrates that tuning the steric bulk of the alkyl chains at the 2,9-positions has a quantifiable effect on τ. In the following sections, we first correlate experimental and computational $E°$s to evaluate potential entatic state contributions. Analyses are then extended to ground state inner sphere reorganization energies (λ_is) for Cu(I/II) redox and, finally, to Cu(I/II) ^{3}MLCT excited state inner sphere relaxation energies (γ_is) and energy gaps. As shown below, entatic energies depend on the model used to quantify them. For Cu-photosentizers, we have determined that excited state relaxation energies provide a means to quantify purely steric contributions to ^{3}MLCT dynamics (*vide infra*).

As pointed out recently for Cu(I) bis-phen complexes,[39] variations in $E°$s and τs reflect the same structural distortion (Figure 4.1); therefore, one can draw a correlation between these experimental observables to quantify entatic contributions to photophysical dynamics. Experimental and calculated $E°$s for Cu(I) bis-phen and the 2,9-alkyl substituted complexes are given in Table 4.1 and Figure 4.6. The best agreement between theory and experimental $E°$s in

DCM is observed for the BP86 functional. Thus, if not specified, calculated values correspond to values obtained using the BP86 exchange correlation functional. Within this functional, the best agreement is observed for the bulkier substituents (e.g., bis-dbp, -dsbp, and -dtbp). For bis-phen and -dmp, however, the calculated *E*°s (1.071 and 1.259 V, respectively) are higher than those observed experimentally (0.84 and 0.99 V, respectively). Furthermore, there is a fairly large *E*° difference between bis-phen and bis-dmp complexes relative to the other complexes with *E*°s reported in the literature (Table 4.1). For a more reliable overall comparison across the series, it is useful to fill this gap. Doing so is also important for analyzing ^{3}MLCT lifetimes and relaxation energies (*vide infra*). We therefore synthesized the homoleptic Cu(I) complex with a 2-methyl-1,10-phenanthroline (mmp) ligand (bis-mmp)[30] and measured its *E*° (0.99 V) and photophysical properties for the first time. Similar to bis-phen and -dmp, the calculated *E*° (1.145 V) is higher than that observed experimentally. We return to this difference below (*vide infra*).

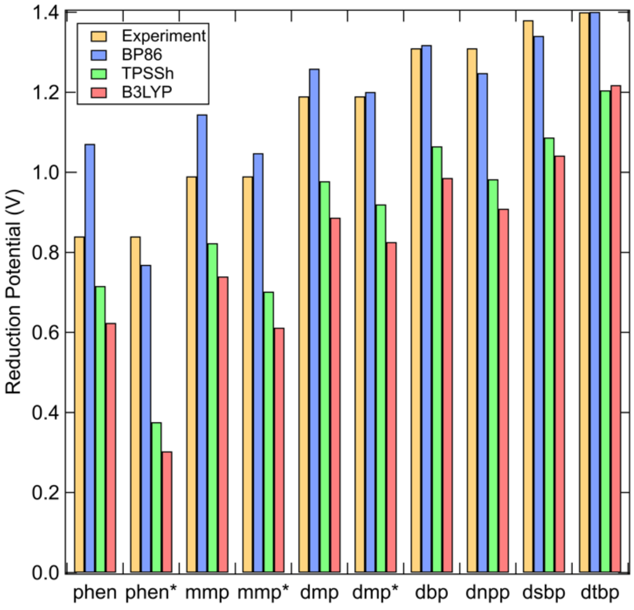

Figure 4.6 Comparison between experimental and calculated *E*°s for phen and 2,9-alkyl substituted complexes.

Table 4.1. Experimental and Calculated *E*°s (V vs. NHE) for 2,9-alkyl substituted bis-phen complexes.

Ligand	BP86 (eV)	TPSSh (eV)	B3LYP (eV)	Experiment (V)	BP86 – Exp. (V)
phen	1.071	0.716	0.624	0.84[a]	0.23
phen*	0.769	0.376	0.303	0.84[a]	-0.07
mmp	1.145	0.823	0.740	0.99[a]	0.16
mmp*	1.048	0.702	0.612	0.99[a]	0.06
dmp	1.259	0.978	0.887	1.19[a]	0.07
dmp*	1.201	0.920	0.826	1.19[a]	0.01
dbp	1.318	1.065	0.987	1.31[b]	0.01
dnpp	1.248	0.983	0.909	1.31[b]	-0.06
dsbp	1.341	1.087	1.042	1.38[b]	-0.04
dmp-dtbp	1.459	1.243	1.197		
dtbp	1.401	1.205	1.218	1.40[c]	0.00

*Optimized structure includes a weak H_2O interaction as discussed in the text.

[a] This work

[b] Ref 34

[c] Ref 38

As discussed above for *E*°, there is a nearly three order of magnitude gap between the τs of bis-phen and bis-dmp complexes (0.14 vs. 90 ns, respectively). We therefore measured the

^{3}MLCT lifetime of bis-mmp in DCM. The absorption data and corresponding transient absorption data for bis-mmp are given in Figures 4.4 and 4.5 (excitation at 410 nm). Fits to the decay of the excited state absorption at 550 nm give a lifetime of 2 ns. Note that the correlations presented in Figures 4.6 and 4.7 below predicted a similar lifetime for bis-mmp *a priori*; this observation points to the predictive and interpretive power of the correlations addressed herein. The latter in particular is elaborated on through comparisons to other Cu(I)-based photosentizers in the Discussion section.

Experimental ln(τ)s are correlated to experimental *E*°s for bis-phen and the 2,9-alkyl substituted Cu(I) complexes in Figure 4.7. Given the broad range of structures, *E*°s, and lifetimes over these seven complexes, this linear correlation can provide a means to estimate an entatic energy. The slope and y-intercept of the correlation between ln(τ) and *E*°, along with the corresponding regression analysis at the 95% confidence interval, provides an entatic energy of 3.2 ± 0.7 kcal/mol (0.14 ± 0.03 eV) for one order of magnitude change in τ. The experimental τs of the complexes considered in Figure 4.7 span many orders of magnitude; translating to this experimental window in ^{3}MLCT lifetime equates to an entatic energy of 12.9 ± 2.9 kcal/mol (0.56 ± 0.13 eV) for a four orders of magnitude change in τ.

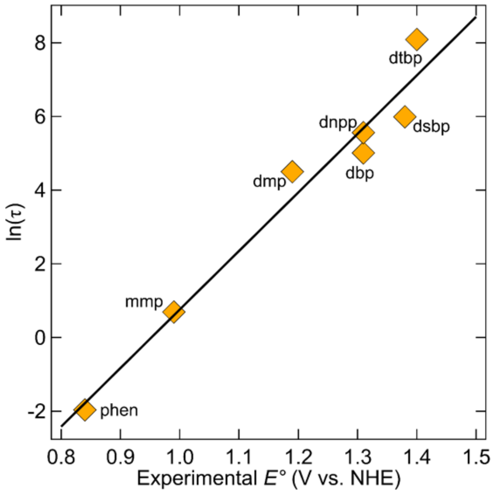

Figure 4.7 The correlation between experimental *E*°s and ln(*τ*)s for bis-phen and 2,9-alkyl substituted Cu(I) complexes. The linear fit has an $R^2 = 0.963$ and the equation $y = (15.89\ V^{-1})x + 15.14$.

While the correlation between *E*° and ln(τ) is a potentially attractive means of determining entatic energies, solvation contributions can affect the Cu(I/II) *E*°. For instance, *E*° for bis-dmp can shift quite dramatically when measured in different coordinating solvents (e.g., a shift of -0.16 or -0.29 V is observed moving from DCM to CH_3CN or DMSO, respectively[31]). This solvent effect was successfully modeled assuming fast, reversible coordination upon oxidation, with little solvent binding to Cu(I).[31] In addition to ground state redox, solvent interactions have also been invoked and discussed for Cu-based excited state ^{3}MLCT formation and decay.[18] In the former case, coordination to Cu(II) stabilizes the oxidized state relative to the reduced state; this differential oxidation state stabilization decreases *E*°. Here, however, focusing solely on noncoordinating DCM allows us to effectively reduce contributions from direct solvent coordination to Cu(II) as much as possible and therefore provide a more accurate quantification of entatic contributions to

E°. Nonetheless, despite being carried out in DCM, the electrochemical data for Cu(I) bis-phen is quasi-reversible, and high scan rates (>600 mV/s) are required. Thus, for the less solvent protected ligand sets, there are likely interactions between the oxidized state and some combination of solvent, electrode surface, and/or counter ion that can potentially contribute to *E*°. However, this selective interaction for Cu(II) is not accounted for using continuum solvation calculations, and we therefore attribute the discrepancies noted above (*vide supra*) between calculated and experimental potentials for bis-phen, -mmp, and -dmp complexes to this differential oxidation state stabilization. Note the deviations between experiment and theoretical *E*°s are 0.23, 0.16, and 0.07 V for bis-phen, -mmp, and -dmp, respectively, supporting the diminished differential oxidation state stabilization across this series as ligand bulk is increased. Importantly, this observation also suggests that solvent contributions can affect the correlation between *E*° and ln(τ), and thus the quantification of entatic contributions. For example, using the computational values of *E*°, which should represent a limit where no differential Cu(II) interactions are present, the correlation between *E*° and ln(τ) gives entatic energies of 1.7 ± 0.5 (0.07 ± 0.02 eV) and 6.8 ± 2.1 kcal/mol (0.29 ± 0.09 eV), respectively, for one and four orders of magnitude change in τ. These values are less than the 3.2 ± 0.7 (0.14 ± 0.03 eV) and 12.9 ± 2.9 kcal/mol (0.56 ± 0.13 eV) using experimental *E*°s (*vide supra*), which further indicates that differential oxidation state stabilization can affect the correlation between *E*° and ln(τ), and thus the entatic energy.

The differential oxidation state interactions can be evaluated by including the effects of a weakly coordinating ligand interaction (H_2O) in Cu bis-phen, -mmp, and -dmp complexes (denoted bis-phen*, -mmp*, and -dmp*). Note the Cu(II)–OH_2 bond in bis-phen* is weak (~2.4 and ~2.5 Å in the oxidized and ^{3}MLCT states, respectively) and significantly weaker in bis-mmp* (~2.9 and ~3.0 Å in bis-mmp*). Water does not bond to Cu(II) in bis-dmp*. Differential oxidation state stabilization in bis-phen* lowers the calculated *E*° (BP86) from 1.07 to 0.77 V vs. NHE (Table 4.1), in better agreement with experiment. Additionally, including the oxidation state selective interactions in bis-mmp* and -dmp* lowers the calculated *E*°s to 1.048 and 1.201 V, respectively, both improved relative to experiment. Lastly, correlating the calculated *E*°s and ln(τ) using these values for bis-phen*, -mmp*, and -dmp* gives entatic energies of 3.3 ± 0.9 (0.14 ± 0.04 eV) and 13.1 ± 3.6 kcal/mol (0.57 ± 0.16 eV) for one and four orders of magnitude change in τ, respectively, in excellent agreement with values from purely experimental *E*°s (*vide supra*).

In addition to sterics, the difference in electron-donating ability of the 2,9-alkyl substituents relative to –H can contribute to *E*° by preferentially stabilizing the oxidized over the reduced state. Here steric vs. electronic contributions can be decomposed using "H–capped" versions of the 2,9-alkyl substituents, which involve replacing the 2,9-alkyl group with an H atom and keeping the geometry completely unperturbed otherwise. Indeed, calculated *E*°s are sensitive to H–capping. For example, for bis-dtbp, -dsbp, and -dmp, the difference in calculated *E*° between H–capped and uncapped structures is 0.148, 0.040, and 0.013 V, respectively, showing a systematic decrease with increasing electron-donating ability across the series. These contributions can also affect the correlation between *E*° and ln(τ). Using the calculated H–capped values and correlating with experimental ln(τ)s results in entatic contributions for one and four orders of magnitude change in τ of 2.2 ± 1.0 (0.10 ± 0.04 eV) and 8.8 ± 4.1 kcal/mol (0.38 ± 0.18 eV), respectively. While the correlation for the H–capped structures is not as tight, these results suggest that the entatic contribution for the H–capped structures is larger than for the uncapped structures and that the electron-donating ability of the alkyl group opposes the entatic state. For a clearer comparison, τ increases from 0.14 to 3260 ns going from bis-phen to bis-dtbp. The calculated *E*°s for these structures vary by 0.330 V (~7.6 kcal/mol) in the uncapped structures. This difference increases to

0.476 V (~11.0 kcal/mol) in the H–capped structures. Therefore, the intrinsic entatic energy from bis-phen to bis-dtbp is opposed by the electron-donating dtbp group, consistent with the analyses using the slope of $E°$ vs. $\ln(\tau)$.

In summary, for this series of Cu photosensitizers, experimental $E°$s correlate linearly with τ over four orders of magnitude in lifetime. The slope of this correlation provides a potential quantitative estimate of the entatic contributions to τ. From experiment, the entatic energy is estimated to be 12.9 ± 2.9 kcal/mol (0.56 ± 0.13 eV) for a four order of magnitude increase in τ. However, differential oxidation state interactions over this series of complexes can affect the correlation and result in an overestimation of the entatic energy. This is exemplified by comparing the entatic energies from calculated $E°$s with and without differential oxidation state interactions (6.8 ± 2.1 kcal/mol (0.29 ± 0.09 eV) and 13.1 ± 3.6 kcal/mol (0.57 ± 0.16 eV), respectively, for a four order of magnitude increase in excited state lifetime). Additionally, steric and electronic contributions to the slope can be decomposed using H–capped vs. uncapped structures. Analyses of these structures indicate that the electron-donating ability of the 2,9-alkyl substituents oppose the entatic contributions to the potentials and lifetimes from sterics; this is exemplified by the bis-phen to bis-dtbp comparison described above, for which the entatic energy is opposed by electron-donation by ~3 kcal/mol (~0.1 eV).

Entatic Contributions and Cu(I/II) Reorganization Energies

Entatic states have been invoked to rationalize the small reorganization energies of biological electron transfer active sites, which for T1 Cu active sites (e.g., plastocyanin, azurin) range from 0.7–1.2 eV.[40,41] This value contains contributions from outer sphere reorganization as well, and the inner sphere contribution is thought to be ~0.4 eV. Here we use λ_is as an alternative means of quantifying entatic contributions to excited state processes, as they better capture the relative curvatures of the potential energy surfaces involved in redox and photophysical processes.

The approach described by Ryde et al.[42,43] has been applied successfully in calculating the λ_is for a wide-range of Cu complexes. Here λ_is have been calculated for a series of bis-phen and 2,9-alkyl Cu(I) complexes (Table 4.2). λ_i for bis-phen is calculated to be 1.06 eV (BP86). For comparison, this value is lower than that reported by Ryde et al. for Cu(I/II)$(NH_3)_4$ (1.40 eV),[42] which reflects the increased steric constraints provided by the phen ligand relative to NH_3. Note the majority of λ_i for Cu(I/II)$(NH_3)_4$ derives from the tetragonal distortion.[41,42] Beyond $E°$, additional insights regarding entatic contributions, including potential energy surfaces and their curvatures, can be determined from ground state λ_is.

As discussed above, a correlation can be drawn between the calculated ground state λ_is and the experimental ln(τ)s. This correlation, given in Figure 4.8A, is also linear and provides entatic contributions for one and four orders of magnitude change in τ of 4.3 ± 0.6 and 17.3 ± 2.2 kcal/mol. These calculated λ_is are free from differential oxidation state contributions, as was evaluated above for redox potentials. For comparison, using bis-phen*, -mmp*, and -dmp* in the correlation provides entatic contributions for one and four orders of magnitude change in τ of 5.4 ± 0.5 and 21.7 ± 2.0 kcal/mol.

Table 4.2 Comparisons between excited state lifetimes and calculated ground state reorganization energies, excited state relaxation energies, and energy gaps for 2,9-alkyl substituted bis-phen complexes.[a]

Ligand	τ (ns)	ln(τ)	λ (eV)[b]	λ (eV)[c]	γ (eV)[b]	γ (eV)[c]	EG (eV)[b]	EG (eV)[c]

phen	0.14	-1.97	0.994 (22.9)	1.064 (24.5)	1.434 (33.1)	1.428 (32.9)	0.778 (17.9)	0.767 (17.7)
phen*			1.067 (24.6)	1.222 (28.2)	1.391 (32.1)	1.411 (32.5)	0.655 (15.1)	0.627 (14.5)
mmp	2[d]	0.69	0.706 (16.3)	0.763 (17.6)	1.114 (25.7)	1.112 (25.6)	1.044 (24.1)	1.029 (23.7)
mmp*			0.802 (18.5)	0.922 (21.3)	1.202 (27.7)	1.202 (27.7)	0.944 (21.8)	0.932 (21.5)
dmp	90	4.50	0.484 (11.2)	0.521 (12.0)	0.910 (21.0)	0.890 (20.5)	1.377 (31.8)	1.360 (31.4)
dmp*			0.481 (11.1)	0.526 (12.1)	0.865 (19.9)	0.867 (20.0)	1.330 (30.7)	1.321 (30.5)
dbp	150	5.01	0.445 (10.3)	0.458 (10.6)	0.747 (17.2)	0.725 (16.7)	1.507 (34.8)	1.507 (34.8)
dnpp	260	5.56	0.388 (9.0)	0.393 (9.1)	0.665 (15.3)	0.664 (15.3)	1.418 (32.7)	1.423 (32.8)
dsbp	400	5.99	0.397 (9.2)	0.407 (9.4)	0.715 (16.5)	0.716 (16.5)	1.511 (34.8)	1.515 (34.9)

dmp-dtbp	730[e]	6.59	0.383 (8.8)	0.381 (8.8)	0.616 (14.2)	0.621 (14.3)	1.658 (38.2)	1.649 (38.0)
dtbp	3260	8.09	0.176 (4.1)	0.183 (4.2)	0.312 (7.2)	0.312 (7.2)	1.896 (43.7)	1.894 (43.7)

*Optimized structure includes a weak H_2O interaction as discussed in the text.

[a] Unless indicated, lifetimes were taken from Table 1 of Ref 21 and references cited therein. Parenthetical values in kcal/mol.

[b] Gas phase.

[c] CPCM corrected.

[d] This work.

[e] Ref 38.

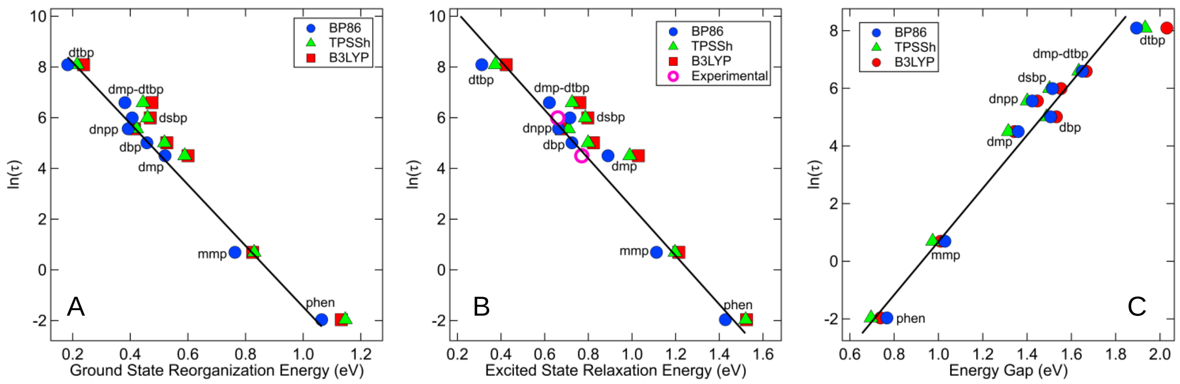

Figure 4.8 Correlations between ln(τ)s and (**A**) ground state reorganization energies, (**B**) excited state relaxation energies, and (**C**) energy gaps for bis-phen and the 2,9-alkyl substituted Cu(I) complexes. The linear fit (black line) is shown for BP86. For A, the fit has $R^2 = 0.984$ and the equation $y = (-12.06\ \mathrm{eV}^{-1})x + 10.59$. For B, $R^2 = 0.956$ and the equation $y = (-9.58\ \mathrm{eV}^{-1})x + 12.05$. For C, $R^2 = 0.965$ and the equation $y = (9.23\ \mathrm{eV}^{-1})x + 8.55$.

As presented above for ground state redox, the λ_is can be corrected for electron-donating effects of the 2,9-alkyl substituents to decompose the steric and electronic contributions to λ_i by analyzing the H-capped structures. The H–capped results provide entatic contributions for one and four orders of magnitude in τ of 4.4 ± 0.7 and 17.7 ± 3.0 kcal/mol. These values are similar to those obtained from uncapped structures, indicating that, unlike E°s, electron-donating effects are minimized in the evaluation of λ_i. Thus, the entatic contributions estimated using λ_i are largely due to sterics and further suggest sterics play a more significant role in excited state lifetimes than electron-donating contributions. This is corroborated below using excited state relaxation energies.

Lastly, entatic contributions estimated for over four orders of magnitude change in τ are similar between gas phase and CPCM solvation approaches (15.7 ± 2.4 and 17.3 ± 2.2 kcal/mol, respectively). This observation further supports that λ_is more so reflect geometric/steric contributions as opposed to solvation and/or electron-donating effects.

In summary, for this series of Cu(I) photosensitizers, the calculated λ_is correlate linearly with $\ln(\tau)$ over four orders of magnitude in τ. The slope of this correlation provides a potential quantitative estimate of the entatic contributions to the excited state lifetimes. The entatic energy using this method is estimated to be 17.3 ± 2.2 kcal/mol for a four order of magnitude increase in τ. In contrast to E°s, differential oxidation state interactions over this series of complexes has a significantly smaller effect on the correlation between energetics and $\ln(\tau)$. Furthermore, electron-donating effects, estimated using the comparison between H–capped and uncapped structures, are minimized in λ_is, which results in similar estimates of entatic contributions.

Entatic Contributions and Cu(I/II) Metal-to-Ligand Charge Transfer Relaxation

In addition to λ_is, the same methodology can be translated to estimate excited state ^{3}MLCT relaxation energies (γ_is). The calculated γ_is are given in Table 4.2, and their correlation with experimental ln(τ) is given in Figure 4.8B. This correlation provides entatic contributions of 5.3 ± 1.1 and 21.2 ± 4.5 kcal/mol, respectively, for one and four orders of magnitude change in τ.

To provide an experimental calibration, 77 K emission spectra were collected on $[Cu(dsbp)_2][PF_6]$ and $[Cu(dmp)_2][PF_6]$ complexes in 1:1 toluene/DCM glasses, and experimental bandwidths and fittings provide γ_is of 0.66 and 0.77 eV, respectively.[44] These values are in fair agreement with those calculated for bis-dsbp and -dmp complexes (0.715 and 0.910 eV, respectively) and are in good agreement with the overall correlation between ln(τ) and γ_i for bis-phen and the 2,9-alkyl complexes (Figure 4.8B, pink circles).

As done above, the potential role of differential solvation can be evaluated using the γ_is estimated for bis-phen*, -mmp*, and -dmp*. Using these structures in the correlation, entatic energies for one and four orders of magnitude in τ are estimated to be 5.5 ± 1.0 and 21.8 ± 4.1 kcal/mol, respectively. Furthermore, the role of electron-donation can be evaluated using the H–capped and uncapped structures. Using the H–capped structures gives entatic contributions of 5.2 ± 1.4 and 20.8 ± 5.5 kcal/mol, respectively, for one and four orders of magnitude change in τ. As with λ_is, γ_is provide very similar entatic contributions using H–capped vs. uncapped structures, both suggesting that excited state lifetimes are largely governed by sterics, and electron-donating contributions from the 2,9-alkyl groups are minimal. Furthermore, entatic contributions over four orders of magnitude in τ are similar between gas phase and PCM solvation approaches (21.3 ± 4.8 and 21.2 ± 4.5 kcal/mol, respectively). This further supports the observation that the calculated γ_is purely reflect geometric and steric contributions to the relaxation energy.

In summary, for this series of Cu photosensitizers, the calculated γ_is correlate linearly with ln(τ) over four orders of magnitude in τ. The slope of this correlation provides a potential quantitative estimate of the entatic contributions. The entatic energy estimated for four orders of magnitude in τ using the uncapped structures (21.2 ± 4.5 kcal/mol) is essentially identical to those determined using H–capped structures (20.8 ± 5.5 kcal/mol) or those accounting for differential oxidation state stabilization (21.8 ± 4.1 kcal/mol). Additionally, gas phase and PCM corrected calculations provide essentially identical entatic contributions. Thus, correlating γ_is and experimental τs provides a robust means to quantify purely geometric and steric contributions from the entatic state. As discussed below, we therefore use this correlation to provide a comparison to a variety of classes of Cu-based photosensitizers reported in the literature.

Entatic Contributions and the Cu(I/II) Metal-to-Ligand Charge Transfer Energy Gap

In addition to λ_is and γ_is, we can apply the same correlation between ln(τ) and the calculated energy gap between the ^{3}MLCT excited state and the reduced ground state in the equilibrium structure of the ^{3}MLCT excited. These energies are reported in Table 2 and are correlated with ln(τ) in Figure 4.8C. This correlation provides entatic contributions of 5.6 ± 1.0 and 22.2 ± 4.2 kcal/mol, respectively, for one and four orders of magnitude change in τ. This is in good agreement with entatic estimates using γ_is.

As done above, the potential role of differential solvation can be evaluated using the energy gaps for bis-phen*, -mmp*, and -dmp*. Using these structures in the correlation, entatic energies for one and four orders of magnitude in τ are estimated to be 6.4 ± 0.9 and 25.6 ± 3.8 kcal/mol, respectively. Furthermore, using the H–capped structures gives entatic contributions of 5.5 ± 1.6

and 22.1 ± 6.2 kcal/mol, respectively, for one and four orders of magnitude change in τ. As with λ_is and γ_is, energy gaps provide very similar entatic contributions using H–capped vs. uncapped structures, both suggesting that excited state lifetimes are largely governed by sterics, and electron-donating contributions from the 2,9-alkyl groups are minimal. Furthermore, entatic contributions over four orders of magnitude in τ are similar between gas phase and PCM solvation approaches (21.9 ± 4.3 and 22.2 ± 4.2 kcal/mol, respectively). This further supports the observation that the calculated λ_is, γ_is, and energy gaps purely reflect geometric and steric contributions to the relaxation energy.

In summary, similar to λ_is and $E°$s, the entatic energetics from the energy gap are somewhat sensitive to differential solvation, whereas γ_is appear to provide entatic energies that reflect steric contributions over this series of Cu bis-phen-based complexes. From these data, the entatic state can provide a strong influence over dynamics that can be described by the energy gap law.

Discussion

Photosensitizers have a broad range of applications, including solar electricity generation, solar fuels catalysis, photoredox catalysis, and OLEDs. Their applicability hinges on excited state lifetimes and excited state redox potentials. In terms of the former, much discussion has revolved around sterics and increasing structural rigidity. For Cu-based photosensitizers, the direct correlation between their excited state structural changes and the ground state redox properties of electron transfer active sites of metalloproteins has inspired an extension of the entatic/rack-induced state to photosensitizer dynamics.[39,45] While a core concept in bioinorganic chemistry and a powerful way to inspire new ligand design, the entatic state is difficult to quantify, and there are only a few examples in the literature where this has been accomplished.[46–50] Here we have leveraged correlations between ^{3}MLCT excited state lifetimes of Cu(I) bis-phen complexes and their corresponding *E*°s, λ_is, γ_is, and energy gaps (Figures 4.8A/B/C, respectively). These linear correlations are observed for over four orders of magnitude change in τ and provide a direct means to quantify entatic state contributions to the excited state dynamics of a broad range of Cu(I)-based photosensitizers.

There can be differences in the quantified entatic energies, however, depending on which correlation is used. A summary of values for different approaches is given in Table 4. When using *E*°s, there can be significant contributions from differential oxidation state stabilization, which, for Cu(I) bis-phen complexes, stabilizes the oxidized over the reduced state and lowers the redox potential. This can affect the correlation between ln(τ) and redox potential. For example, from Table 4, the correlation between ln(τ) and experimental redox potential provides an estimate of an entatic contribution of 12.9 ± 2.9 kcal/mol for a four order of magnitude change in τ, while the same correlation using calculated values of redox potentials gives 6.8 ± 2.1 kcal/mol. The difference between these values largely derives from the overestimation of the calculated *E*°s of bis-phen, -mmp, and -dmp complexes. This overestimation decreases the slope of the ln(τ)/*E*° correlation and gives rise to a lower value of entatic energy. Above, it was shown that accounting for the differential oxidation state stabilization for the three complexes (using bis-phen*, -mmp*, and -dmp*) results in a slope of 13.1 ± 3.6 kcal/mol, in much better agreement with experiment. Lastly, by using H–capped structures, it was demonstrated that electron donating effects of the 2,9-alkyl substituents can oppose the entatic state contributions (e.g., by ~3 kcal/mol for bis-phen vs. bis-dtbp).

Table 4.3. Entatic state analyses.[a]

Method	**R^2**	**slope (eV)**	**y-int (eV)**	**Entatic (kcal/mol)[b]**	**Entatic (kcal/mol)[c]**
$E°$ (1)[d]	0.963	0.0606	0.9616	3.2 ± 0.7	12.9 ± 2.9
$E°$ (2)[e]	0.935	0.0322	1.1264	1.7 ± 0.5	6.8 ± 2.1
$E°$ (3)[f]	0.946	0.0616	0.9440	3.3 ± 0.9	13.1 ± 3.6
$E°$ (4)[g]	0.857	0.0414	1.1243	2.2 ± 1.0	8.8 ± 4.1
λ_i (1)[h]	0.984	-0.0816	0.0873	4.3 ± 0.6	17.3 ± 2.2
λ_i (2)[i]	0.992	-0.1020	1.0010	5.4 ± 0.5	21.7 ± 2.0
λ_i (3)[j]	0.972	-0.0832	0.8817	4.4 ± 0.7	17.7 ± 3.0
λ_i (4)[k]	0.977	-0.0740	0.8156	3.9 ± 0.6	15.7 ± 2.4
γ_i (1)[h]	0.956	-0.0998	1.2383	5.3 ± 1.1	21.2 ± 4.5
γ_i (2)[i]	0.966	-0.1027	1.2571	5.5 ± 1.0	21.8 ± 4.1
γ_i (3)[j]	0.934	-0.0979	1.2378	5.2 ± 1.4	20.8 ± 5.5
γ_i (4)[k]	0.952	-0.1002	1.2461	5.3 ± 1.2	21.3 ± 4.8
EG (1)[h]	0.965	0.1046	0.9424	5.6 ± 1.0	22.2 ± 4.2
EG (2)[i]	0.978	0.1205	0.8395	6.4 ± 0.9	25.6 ± 3.8
EG (3)[j]	0.926	0.1043	0.9172	5.5 ± 1.6	22.1 ± 6.2

EG (4)[k]	0.962	0.1032	0.9539	5.5 ± 1.1	21.9 ± 4.3

[a] Error analyses conducted at the 95% confidence interval.

[b] One order of magnitude change in τ.

[c] Four orders of magnitude change in τ.

[d] Using experimental *E*°s.

[e] Using calculated *E*°s (uncapped).

[f] Using calculated *E*°s with differential oxidation state stabilization (bis-phen*, -mmp*, and -dmp*). *Optimized structure includes a weak H_2O interaction as discussed in the text.

[g] Using calculated *E*°s (H–capped).

[h] Using calculated energies (uncapped).

[i] Using calculated energies with differential oxidation state stabilization (bis-phen*, -mmp*, and -dmp*).

[j] Using calculated energies (H–capped).

[k] Using calculated energies (uncapped, gas phase).

Overall, the sensitivity to differential oxidation state contributions, largely stemming from the fact that the total oxidation state changes during redox (i.e. Cu(I/II)), in addition to contributions from electron-donating/-withdrawing effects of the 2,9-alkyl groups, suggests that using the correlation between *E*° and ln(τ) is not an ideal way to quantify entatic states in photophysical processes. This is perhaps not surprising given that ground state potentials are thermodynamic quantities and do not take into account important contributions from shifts and changes in curvature of the excited state potential energy surfaces when an entatic state is present.

The extension of the correlation to λ_is alleviates some of the issues presented using *E*°s. The entatic energies estimated using the correlations with calculated λ_is are also given in Table 4. Here the correlation provides an entatic energy of 17.3 ± 2.2 kcal/mol, and differential oxidation state stabilization using bis-phen*, -mmp*, and -dmp* provides an entatic energy that varies less relative to the same comparison using redox potentials (21.7 ± 2.0). Additionally, the entatic energy is not sensitive to electron-donating/-withdrawing effects (i.e. H–capped vs. capped, 17.3 ± 2.2 vs. 17.7 ± 3.0 kcal/mol, respectively). These observations are also mirrored by the use of calculated γ_is, which provide an entatic energy of 21.2 ± 4.5 kcal/mol for a four order of magnitude change in τ. This value is similar when incorporating differential oxidation state stabilization, H–capped vs. uncapped structures, or gas phase vs. PCM calculations (Table 4.3), which indicates it is a robust, general means to estimate entatic contributions to photophysical processes. This correlation is used below to quantify entatic energies across other types of Cu(I)-based photosensitizers.

Conclusion

This study has developed a combined experimental and computational methodology to quantify entatic contributions to photophysical processes, with specific applications to a broad range of Cu-based photosensitizers and luminescent complexes. This methodology is based on the observation that experimental ^{3}MLCT excited state lifetimes for a range of Cu(I) bis-phen complexes correlate with redox potentials, ground state inner sphere reorganization energies, and excited state relaxation energies and energy gaps over four orders in magnitude in time. These correlations provide a means to directly quantify entatic contributions to the ^{3}MLCT excited state lifetimes over an entire class of photoactive metal complexes. Furthermore, the correlations in Figure 4.8 provide a means to benchmark the potential performance characteristics of new complexes before embarking on their syntheses. Lastly, within Cu(I)-based photosensitizers, entatic states are found here to reach ~20 kcal/mol relative to the conformationally flexible $[Cu(phen)_2]^+$. Being the largest entatic states yet quantified, these energetics are significant relative to typical chemical driving forces and barriers, suggesting entatic state descriptors will be valuable to extend to new classes of molecules and materials with interesting functional properties involving the coupling between electron and vibrational dynamics. Our laboratory is currently extending these analyses to quantifying entatic states in (photo)catalytic and (photo)magnetic materials.

Citations

(1) Lumry, R.; Eyring, H. Conformation Changes of Proteins. *J. Phys. Chem.* **1954**, *58* (2), 110–120. https://doi.org/10.1021/j150512a005.

(2) Vallee, B. L.; Williams, R. J. Metalloenzymes: The Entatic Nature of Their Active Sites. *Proceedings of the National Academy of Sciences* **1968**, *59* (2), 498–505. https://doi.org/10.1073/pnas.59.2.498.

(3) Williams, R. J. P. Energised (Entatic) States of Groups and of Secondary Structures in Proteins and Metalloproteins. *European Journal of Biochemistry* **1995**, *234* (2), 363–381. https://doi.org/10.1111/j.1432-1033.1995.363_b.x.

(4) Gray, H. B.; Malmström, Bo. G. On the Relationship between Protein-Forced Ligand Fields and the Properties of Blue Copper Centers. *Comments on Inorganic Chemistry* **1983**, *2* (5), 203–209. https://doi.org/10.1080/02603598308078118.

(5) Malmström, B. G. Rack-Induced Bonding in Blue-Copper Proteins. In *EJB Reviews 1994*; Christen, P., Hofmann, E., Eds.; Springer: Berlin, Heidelberg, 1995; pp 157–164. https://doi.org/10.1007/978-3-642-79502-2_12.

(6) Gray, H. B.; Malmström, B. G.; Williams, R. J. P. Copper Coordination in Blue Proteins. *J. Biol. Inorg. Chem.* **2000**, *5* (5), 551–559. https://doi.org/10.1007/s007750000146.

(7) Ghosh, S.; Xie, X.; Dey, A.; Sun, Y.; Scholes, C. P.; Solomon, E. I. Thermodynamic Equilibrium between Blue and Green Copper Sites and the Role of the Protein in Controlling Function. *Proceedings of the National Academy of Sciences* **2009**, *106* (13), 4969–4974. https://doi.org/10.1073/pnas.0900995106.

(8) Mara, M. W.; Hadt, R. G.; Reinhard, M. E.; Kroll, T.; Lim, H.; Hartsock, R. W.; Alonso-Mori, R.; Chollet, M.; Glownia, J. M.; Nelson, S.; Sokaras, D.; Kunnus, K.; Hodgson, K. O.; Hedman, B.; Bergmann, U.; Gaffney, K. J.; Solomon, E. I. Metalloprotein Entatic Control of Ligand-Metal Bonds Quantified by Ultrafast x-Ray Spectroscopy. *Science* **2017**, *356* (6344), 1276–1280. https://doi.org/10.1126/science.aam6203.

(9) Solomon, E. I.; Hadt, R. G. Recent Advances in Understanding Blue Copper Proteins. *Coordination Chemistry Reviews* **2011**, *255* (7), 774–789. https://doi.org/10.1016/j.ccr.2010.12.008.

(10) Hadt, R. G.; Xie, X.; Pauleta, S. R.; Moura, I.; Solomon, E. I. Analysis of Resonance Raman Data on the Blue Copper Site in Pseudoazurin: Excited State π and σ Charge Transfer Distortions and Their Relation to Ground State Reorganization Energy. *Journal of Inorganic Biochemistry* **2012**, *115*, 155–162. https://doi.org/10.1016/j.jinorgbio.2012.03.006.

(11) Rorabacher, D. B. Electron Transfer by Copper Centers. *Chem. Rev.* **2004**, *104* (2), 651–698. https://doi.org/10.1021/cr020630e.

(12) Chaka, G.; Sonnenberg, J. L.; Schlegel, H. B.; Heeg, M. J.; Jaeger, G.; Nelson, T. J.; Ochrymowycz, L. A.; Rorabacher, D. B. A Definitive Example of a Geometric “Entatic State” Effect: Electron-Transfer Kinetics for a Copper(II/I) Complex Involving A

Quinquedentate Macrocyclic Trithiaether−Bipyridine Ligand. *J. Am. Chem. Soc.* **2007**, *129* (16), 5217–5227. https://doi.org/10.1021/ja068960u.

(13) Xie, B.; Elder, T.; Wilson, L. J.; Stanbury, D. M. Internal Reorganization Energies for Copper Redox Couples: The Slow Electron-Transfer Reactions of the [CuII/I(Bib)2]2+/+ Couple. *Inorg. Chem.* **1999**, *38* (1), 12–19. https://doi.org/10.1021/ic980926w.

(14) Comba, P. Coordination Compounds in the Entatic State. *Coordination Chemistry Reviews* **2000**, *200–202*, 217–245. https://doi.org/10.1016/S0010-8545(00)00265-4.

(15) Comba, P. Strains and Stresses in Coordination Compounds. *Coordination Chemistry Reviews* **1999**, *182* (1), 343–371. https://doi.org/10.1016/S0010-8545(98)00199-4.

(16) Lazorski, M. S.; Castellano, F. N. Advances in the Light Conversion Properties of Cu(I)-Based Photosensitizers. *Polyhedron* **2014**, *82*, 57–70. https://doi.org/10.1016/j.poly.2014.04.060.

(17) Lockard, J. V.; Kabehie, S.; Zink, J. I.; Smolentsev, G.; Soldatov, A.; Chen, L. X. Influence of Ligand Substitution on Excited State Structural Dynamics in Cu(I) Bisphenanthroline Complexes. *J. Phys. Chem. B* **2010**, *114* (45), 14521–14527. https://doi.org/10.1021/jp102278u.

(18) Mara, M. W.; Fransted, K. A.; Chen, L. X. Interplays of Excited State Structures and Dynamics in Copper(I) Diimine Complexes: Implications and Perspectives. *Coordination Chemistry Reviews* **2015**, *282–283*, 2–18. https://doi.org/10.1016/j.ccr.2014.06.013.

(19) Capano, G.; Milne, C. J.; Chergui, M.; Rothlisberger, U.; Tavernelli, I.; Penfold, T. J. Probing Wavepacket Dynamics Using Ultrafast X-Ray Spectroscopy. *J. Phys. B: At. Mol. Opt. Phys.* **2015**, *48* (21), 214001. https://doi.org/10.1088/0953-4075/48/21/214001.

(20) Iwamura, M.; Takeuchi, S.; Tahara, T. Real-Time Observation of the Photoinduced Structural Change of Bis(2,9-Dimethyl-1,10-Phenanthroline)Copper(I) by Femtosecond Fluorescence Spectroscopy: A Realistic Potential Curve of the Jahn−Teller Distortion. *J. Am. Chem. Soc.* **2007**, *129* (16), 5248–5256. https://doi.org/10.1021/ja069300s.

(21) Khnayzer, R. S.; McCusker, C. E.; Olaiya, B. S.; Castellano, F. N. Robust Cuprous Phenanthroline Sensitizer for Solar Hydrogen Photocatalysis. *J. Am. Chem. Soc.* **2013**, *135* (38), 14068–14070. https://doi.org/10.1021/ja407816f.

(22) Kohler, L.; Hadt, R. G.; Hayes, D.; Chen, L. X.; Mulfort, K. L. Synthesis, Structure, and Excited State Kinetics of Heteroleptic Cu(I) Complexes with a New Sterically Demanding Phenanthroline Ligand. *Dalton Trans.* **2017**, *46* (38), 13088–13100. https://doi.org/10.1039/C7DT02476B.

(23) Shaw, G. B.; Grant, C. D.; Shirota, H.; Castner, E. W.; Meyer, G. J.; Chen, L. X. Ultrafast Structural Rearrangements in the MLCT Excited State for Copper(I) Bis-Phenanthrolines in Solution. *J. Am. Chem. Soc.* **2007**, *129* (7), 2147–2160. https://doi.org/10.1021/ja067271f.

(24) McCullough, B. J.; Neyhouse, B. J.; Schrage, B. R.; Reed, D. T.; Osinski, A. J.; Ziegler, C. J.; White, T. A. Visible-Light-Driven Photosystems Using Heteroleptic Cu(I) Photosensitizers and Rh(III) Catalysts To Produce H2. *Inorg. Chem.* **2018**, *57* (5), 2865–2875. https://doi.org/10.1021/acs.inorgchem.7b03273.

(25) Dicke, B.; Hoffmann, A.; Stanek, J.; Rampp, M. S.; Grimm-Lebsanft, B.; Biebl, F.; Rukser, D.; Maerz, B.; Göries, D.; Naumova, M.; Biednov, M.; Neuber, G.; Wetzel, A.; Hofmann, S. M.; Roedig, P.; Meents, A.; Bielecki, J.; Andreasson, J.; Beyerlein, K. R.; Chapman, H. N.; Bressler, C.; Zinth, W.; Rübhausen, M.; Herres-Pawlis, S. Transferring

the Entatic-State Principle to Copper Photochemistry. *Nature Chem* **2018**, *10* (3), 355–362. https://doi.org/10.1038/nchem.2916.

(26) Robinson, G. W.; Frosch, R. P. Theory of Electronic Energy Relaxation in the Solid Phase. *J. Chem. Phys.* **1962**, *37* (9), 1962–1973. https://doi.org/10.1063/1.1733413.

(27) Jortner, J. Radiationless Transitions. *Pure and Applied Chemistry* **1971**, *27* (3), 389–420. https://doi.org/10.1351/pac197127030389.

(28) Pallenberg, A. J.; Koenig, K. S.; Barnhart, D. M. Synthesis and Characterization of Some Copper(I) Phenanthroline Complexes. *Inorg. Chem.* **1995**, *34* (11), 2833–2840. https://doi.org/10.1021/ic00115a009.

(29) Ruthkosky, M.; Castellano, F. N.; Meyer, G. J. Photodriven Electron and Energy Transfer from Copper Phenanthroline Excited States. *Inorg. Chem.* **1996**, *35* (22), 6406–6412. https://doi.org/10.1021/ic960503z.

(30) Desvergnes-Breuil, V.; Hebbe, V.; Dietrich-Buchecker, C.; Sauvage, J.-P.; Lacour, J. NMR Evaluation of the Configurational Stability of Cu(I) Complexes. *Inorg. Chem.* **2003**, *42* (2), 255–257. https://doi.org/10.1021/ic0259890.

(31) Scaltrito, D. V.; Thompson, D. W.; O’Callaghan, J. A.; Meyer, G. J. MLCT Excited States of Cuprous Bis-Phenanthroline Coordination Compounds. *Coordination Chemistry Reviews* **2000**, *208* (1), 243–266. https://doi.org/10.1016/S0010-8545(00)00309-X.

(32) Elgrishi, N.; Rountree, K. J.; McCarthy, B. D.; Rountree, E. S.; Eisenhart, T. T.; Dempsey, J. L. A Practical Beginner’s Guide to Cyclic Voltammetry. *J. Chem. Educ.* **2018**, *95* (2), 197–206. https://doi.org/10.1021/acs.jchemed.7b00361.

(33) Noviandri, I.; Brown, K. N.; Fleming, D. S.; Gulyas, P. T.; Lay, P. A.; Masters, A. F.; Phillips, L. The Decamethylferrocenium/Decamethylferrocene Redox Couple: A Superior Redox Standard to the Ferrocenium/Ferrocene Redox Couple for Studying Solvent Effects on the Thermodynamics of Electron Transfer. *J. Phys. Chem. B* **1999**, *103* (32), 6713–6722. https://doi.org/10.1021/jp991381+.

(34) Eggleston, M. K.; McMillin, D. R.; Koenig, K. S.; Pallenberg, A. J. Steric Effects in the Ground and Excited States of Cu(NN)2+ Systems. *Inorg. Chem.* **1997**, *36* (2), 172–176. https://doi.org/10.1021/ic960698a.

(35) Cunningham, C. T.; Cunningham, K. L. H.; Michalec, J. F.; McMillin, D. R. Cooperative Substituent Effects on the Excited States of Copper Phenanthrolines. *Inorg. Chem.* **1999**, *38* (20), 4388–4392. https://doi.org/10.1021/ic9906611.

(36) Ichinaga, A. K.; Kirchhoff, J. R.; McMillin, D. R.; Dietrich-Buchecker, C. O.; Marnot, P. A.; Sauvage, J. P. Charge-Transfer Absorption and Emission of Cu(NN)2+ Systems. *Inorg. Chem.* **1987**, *26* (25), 4290–4292. https://doi.org/10.1021/ic00272a030.

(37) Vögtle, F.; Lüer, I.; Balzani, V.; Armaroli, N. Endoreceptors with Convergent Phenanthroline Units: A Molecular Cavity for Six Guest Molecules. *Angewandte Chemie International Edition in English* **1991**, *30* (10), 1333–1336. https://doi.org/10.1002/anie.199113331.

(38) Green, O.; Gandhi, B. A.; Burstyn, J. N. Photophysical Characteristics and Reactivity of Bis(2,9-Di-Tert-Butyl-1,10-Phenanthroline)Copper(I). *Inorg. Chem.* **2009**, *48* (13), 5704–5714. https://doi.org/10.1021/ic802361q.

(39) Kohler, L.; Hadt, R. G.; Hayes, D.; Chen, L. X.; Mulfort, K. L. Synthesis, Structure, and Excited State Kinetics of Heteroleptic Cu(I) Complexes with a New Sterically Demanding Phenanthroline Ligand. *Dalton Trans.* **2017**, *46* (38), 13088–13100. https://doi.org/10.1039/C7DT02476B.

(40) Di Bilio, A. J.; Hill, M. G.; Bonander, N.; Karlsson, B. G.; Villahermosa, R. M.; Malmström, B. G.; Winkler, J. R.; Gray, H. B. Reorganization Energy of Blue Copper: Effects of Temperature and Driving Force on the Rates of Electron Transfer in Ruthenium- and Osmium-Modified Azurins. *J. Am. Chem. Soc.* **1997**, *119* (41), 9921–9922. https://doi.org/10.1021/ja971518e.

(41) Solomon, E. I.; Szilagyi, R. K.; DeBeer George, S.; Basumallick, L. Electronic Structures of Metal Sites in Proteins and Models: Contributions to Function in Blue Copper Proteins. *Chem. Rev.* **2004**, *104* (2), 419–458. https://doi.org/10.1021/cr0206317.

(42) Olsson, M. H. M.; Ryde, U.; Roos, B. O. Quantum Chemical Calculations of the Reorganization Energy of Blue-Copper Proteins. *Protein Science* **1998**, *7* (12), 2659–2668. https://doi.org/10.1002/pro.5560071220.

(43) Ryde, U.; Olsson, M. H. M. Structure, Strain, and Reorganization Energy of Blue Copper Models in the Protein. *International Journal of Quantum Chemistry* **2001**, *81* (5), 335–347. https://doi.org/10.1002/1097-461X(2001)81:5<335::AID-QUA1003>3.0.CO;2-Q.

(44) Murtaza, Z.; Graff, D. K.; Zipp, A. P.; Worl, L. A.; Jones, W. E. Jr.; Bates, W. D.; Meyer, T. J. Energy Transfer in the Inverted Region: Calculation of Relative Rate Constants by Emission Spectral Fitting. *J. Phys. Chem.* **1994**, *98* (41), 10504–10513. https://doi.org/10.1021/j100092a020.

(45) Dicke, B.; Hoffmann, A.; Stanek, J.; Rampp, M. S.; Grimm-Lebsanft, B.; Biebl, F.; Rukser, D.; Maerz, B.; Göries, D.; Naumova, M.; Biednov, M.; Neuber, G.; Wetzel, A.; Hofmann, S. M.; Roedig, P.; Meents, A.; Bielecki, J.; Andreasson, J.; Beyerlein, K. R.; Chapman, H. N.; Bressler, C.; Zinth, W.; Rübhausen, M.; Herres-Pawlis, S. Transferring the Entatic-State Principle to Copper Photochemistry. *Nature Chemistry* **2018**, *10* (3), 355–362. https://doi.org/10.1038/nchem.2916.

(46) Ghosh, S.; Xie, X.; Dey, A.; Sun, Y.; Scholes, C. P.; Solomon, E. I. Thermodynamic Equilibrium between Blue and Green Copper Sites and the Role of the Protein in Controlling Function. *PNAS* **2009**, *106* (13), 4969–4974. https://doi.org/10.1073/pnas.0900995106.

(47) Tsai, M.-L.; Hadt, R. G.; Marshall, N. M.; Wilson, T. D.; Lu, Y.; Solomon, E. I. Axial Interactions in the Mixed-Valent CuA Active Site and Role of the Axial Methionine in Electron Transfer. *PNAS* **2013**, *110* (36), 14658–14663. https://doi.org/10.1073/pnas.1314242110.

(48) Mara, M. W.; Hadt, R. G.; Reinhard, M. E.; Kroll, T.; Lim, H.; Hartsock, R. W.; Alonso-Mori, R.; Chollet, M.; Glownia, J. M.; Nelson, S.; Sokaras, D.; Kunnus, K.; Hodgson, K. O.; Hedman, B.; Bergmann, U.; Gaffney, K. J.; Solomon, E. I. Metalloprotein Entatic Control of Ligand-Metal Bonds Quantified by Ultrafast x-Ray Spectroscopy. *Science* **2017**, *356* (6344), 1276–1280. https://doi.org/10.1126/science.aam6203.

(49) Metz, M.; Solomon, E. I. Dioxygen Binding to Deoxyhemocyanin: Electronic Structure and Mechanism of the Spin-Forbidden Two-Electron Reduction of O2. *J. Am. Chem. Soc.* **2001**, *123* (21), 4938–4950. https://doi.org/10.1021/ja004166b.

(50) Hadt, R. G.; Xie, X.; Pauleta, S. R.; Moura, I.; Solomon, E. I. Analysis of Resonance Raman Data on the Blue Copper Site in Pseudoazurin: Excited State π and σ Charge Transfer Distortions and Their Relation to Ground State Reorganization Energy. *Journal of Inorganic Biochemistry* **2012**, *115*, 155–162. https://doi.org/10.1016/j.jinorgbio.2012.03.006.